Materials Science and Technology

ISSN: 0267-0836 (Print) 1743-2847 (Online) Journal homepage: http://www.tandfonline.com/loi/ymst20

Assessment of the austemperability of high-silicon cast steels through Jominy hardenability tests

Nicolás Emanuel Tenaglia, Roberto Enrique Boeri, Juan Miguel Massone & Alejandro Daniel Basso

To cite this article: Nicolás Emanuel Tenaglia, Roberto Enrique Boeri, Juan Miguel Massone & Alejandro Daniel Basso (2018): Assessment of the austemperability of high-silicon cast steels through Jominy hardenability tests, Materials Science and Technology, DOI: 10.1080/02670836.2018.1507124

To link to this article: https://doi.org/10.1080/02670836.2018.1507124

Published online: 14 Aug 2018.

MATERIALS SCIENCE AND TECHNOLOGY
https://doi.org/10.1080/02670836.2018.1507124

The Institute of Materials, Minerals and Mining

Taylor & Francis
Taylor & Francis Group

Assessment of the austemperability of high-silicon cast steels through Jominy hardenability tests

Nicolás Emanuel Tenaglia, Roberto Enrique Boeri, Juan Miguel Massone and Alejandro Daniel Basso

Metallurgy Division, INTEMA – CONICET, University of Mar del Plata, Mar del Plata, Argentina

ABSTRACT

The austemperability of seven high silicon cast steels with different alloy contents was characteri sed. The maximum round bar diameter that can be fully austempered changed from about 10 mm for an unalloyed steel to more than 70 mm for a low-alloy steel. The austemperability was calculated by applying a procedure based on a standard Jominy test and the characterisation of the microstructure along the Jominy sample. The method, which was validated experimentally, creates a relatively simple procedure to measure austemperability. Processing factors such as the ability of the salt bath to extract heat and the austempering temperature are accounted for the method. The metallographic study revealed the influence of microsegregation on hardenability, which is particularly important for cast steels.

ARTICLE HISTORY
Received 30 April 2018
Revised 26 July 2018
Accepted 27 July 2018

KEYWORDS
Cast steels; high silicon; hardenability; austemperability; carbide-free bainite

Introduction

In the recent decades, there have been some remarkable advances in the steels engineering driven by the challenges posed by the pressure to produce safety pieces at low cost. One of the most interesting advances in this area has been the development of high silicon bainitic steels, which are carbide-free [1–7]. Carbide-free bainite has been accepted as a variant of bainite and consists of bainitic ferrite subunits (α_B) surrounded by retained austenite (γ), as shown in Figure 1. The high silicon content present in the chemical composition of the steels (at least 1.5 wt-%) retards the carbide precipitation during the bainite transformation and the carbon rejected by ferrite subunits enriches the surrounding austenite, decreasing its M_S (martensite start) temperature and stabilising it at room temperature [7]. This kind of microstructure can achieve great mechanical properties [1,4,8–10].

Carbide-free bainite is commonly obtained by an isothermal heat treatment called 'austempering', schematised in Figure 2(A). The heat treatment consists o f a full austenitising followed by an isothermal cycle, commonly performed in a molten salt bath held at a defined temperature (T_{IB} – temperature of the isothermal bath).

The hardenability of iron-base alloys must be known when quenched and tempered steel parts are produced. The procedure to determine hardenability is described in ASTM A255 standard and it is known as the 'Jominy end-quench test'. Nevertheless, for the case of steels that will undergo an austempering heat treatment in order to obtain a bainitic structure, austemperability is the correct property that should be measured when the maximum part size to be heat-treated properly needs to be quantified.

Austemperability is similar to hardenability, but instead of referring to the ability of the steel to obtain a martensitic microstructure through quenching, for the case of austemperability, it quantifies the aptitude of the steel to achieve a bainitic structure after an isothermal heat treatment. Both hardenability and austemperability are controlled by the chemical composition of the steel and other metallurgical factors. Different from hardenability, there is not a standard specification to determine the austemperability of an iron-base alloy. In fact, the austemperability is not just a property of the alloy, because it depends on several factors, such as the characteristics of the salt bath where the sample is going to be quenched and isothermally maintained during a suitable time. Among others, the main characteristics of a salt bath that can affect its capacity to remove heat from the heat-treated part include its chemical composition, temperature, and water content [11].

The way in which hardenability and austemperability are defined are analogous, since both terms take into account the ability of an alloy to avoid high-temperature transformation products of the austenite, when it cools down from the austenitising temperature until Ms (in the case of hardenability) or until T_{IB} (in the case of austemperability). In both cases, the cooling rate of the entire sample needs to be greater than the

CONTACT Nicolás Emanuel Tenaglia ntenaglia@fi.mdp.edu.ar Metallurgy Division, INTEMA – CONICET, University of Mar del Plata, Colon Av. 10850, Mar del Plata 7600, Argentina

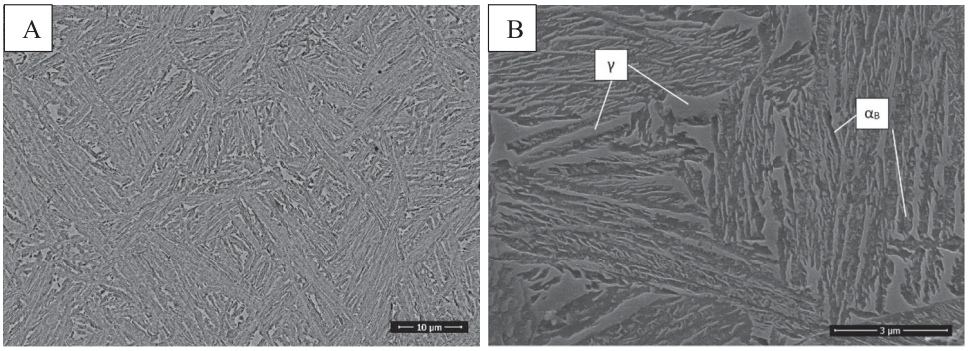

Figure 1. Carbide-free bainitic microstructure at different magnifications.

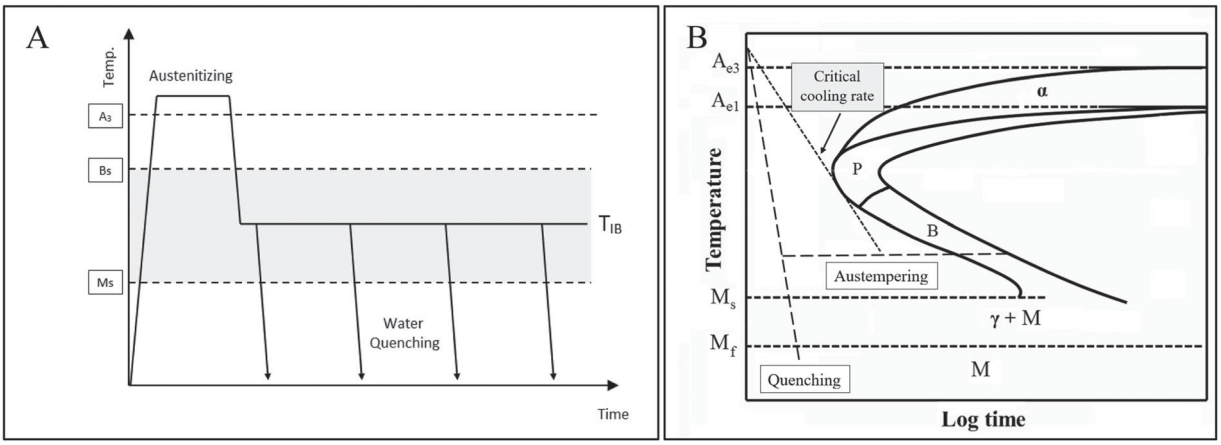

Figure 2. Austempering heat treatment scheme (A). Schematic continuous cooling transformation (CCT) diagram (B).

critical cooling rate to avoid pearlitic or proeutectoid ferrite transformation, as shown in Figure 2(B).

The common procedure to measure the austemperability of an iron-based alloy on a given cooling media involves preparing cylindrical rods of different diameters, performing an austempering heat treatment and measuring, through microstructural observation, the maximum rod diameter able to obtain a fully bainitic microstructure along its entire section [11]. This procedure implies a very tedious and time-consuming experimental work.

Voigt et al. [11] developed a relationship between hardenability and austemperability for cast iron. The study compares the hardenability calculated from chemical composition and experimental data from the literature on the maximum section size that can be successfully austempered for over 30 grades of cast iron of different chemical compositions. The main conclusion of the work is that there is a good correlation between the Jominy distance (D_j) corresponding to the precipitation of high-temperature structures (pearlite, proeutectoid ferrite) and the maximum austemperable diameter. Therefore, in cast iron, it is possible to determine the austemperability by performing a standard Jominy end-quench test.

To the best of our knowledge, there is very limited reference about the austemperability of high silicon steels [12,13]. In fact, most of the studies of carbide-free bainitic steels have been carried out on thin section samples of wrought steels [1–11,14–17]. Just a limited number of works have been focused on cast steels [18–23], but the austemperability of these alloys was not analysed. On the other hand, the austemperability of cast iron has been widely studied [11], since this kind of material is usually austempered to produce 'austempered ductile iron' (ADI), an extensively used material for structural purposes with attractive mechanical properties and low manufacturing cost [18]. The matrix microstructure of ADI is similar to that of carbide-free bainitic steels and consists of a mixture of bainitic ferrite and high-carbon austenite. Unfortunately, the results obtained for the austemperability of ADI cannot be used in carbide-free bainitic cast steels because the presence of graphite nodules and the higher carbon content of ADI matrix introduce substantial differences with respect to steels.

The main objective of this work is to characterise the austemperability of seven high silicon cast steels with different chemical compositions, paying special attention to the influence of some alloy elements and the microsegregation caused during solidification. For that purpose, a procedure to determine the austemperability of steels by means of a standard Jominy end-quench test will be investigated.

Experimental procedure

Design of melts

The cast steels were prepared in an industrial foundry using a medium frequency induction furnace of 80 kg capacity. Selected steel scrap and ferroalloys were used as raw materials. The melts were poured into keel-block-shaped sand moulds (ASTM A703). The chemical compositions of the steels are listed in Table 1 and were determined by using a Baird DV6 spectrometer. Si content was measured by the gravimetric method and C by combustion according to ASTM D350 standard.

The first series of melts, steels 1 to 4, are medium-C steels showing different levels of alloying besides about 2 wt-% Si. Cr, Ni and Mo were added to increase the hardenability. On the other hand, Al and Co were added as they are reported to accelerate the bainitic transformation [24]. The second set of melts include different levels of Cr and higher C contents, since this makes it possible to perform austempering heat treatments at lower temperatures, in agreement with the latest works focused on the austempering of high silicon steels [4,5,8,15–17]. Table 1 also lists Bs and Ms temperatures for the studied steel, which were calculated using a procedure developed by Mathew Peet and H.K.D.H. Bhadeshia (www.msm.cam.ac.uk/map/steel/programs/mucg83.html).

Hardenability evaluation

The Jominy end-quench test (ASTM A255) was applied for the hardenability evaluation. Austeniti sing temperatures followed the instructions of the standard, but an overheating of 40°C was used in all cases, since the microsegregation found in these cast steels can cause that some portions of the matrix to show higher A_{c3} temperatures. After performing the Jominy tests, hardness in Rockwell C scale (HRC) was measured in ground flats along the length of the sample to obtain the Jominy curves. Later, the ground planes were polished and etched with nital (2%) for the metallographic observation. In addition to the Jominy hardness plot, the distance from the end-quench that shows the presence of undesired phases (different from martensite) was identified by means of metallographic observation and called D_{jm}. This procedure is particularly useful when the hardness plot shows relatively small changes as a function of Jominy distance. The metallographic observation identifies the critical cooling rate for the precipitation of unwanted phases with better accuracy. This procedure was already reported by Fernandino et al. for cast iron [25].

Table 1. Chemical composition (wt-%), Bs and Ms temperatures (°C) of the cast steels.

	C	Si	Mn	Cr	Ni	Mo	Al	Co	Bs	Ms
S1	0.45	2.13	0.60	0.024	0.003	0.002	0.034	0.002	515	305
S2	0.54	2.01	0.64	0.50	0.003	0.007	0.042	0.002	485	269
S3	0.40	2.06	0.59	0.52	0.49	0.53	0.035	0.002	503	280
S4	0.43	2.06	0.58	0.59	0.56	0.53	0.61	0.21	519	285
S5	0.71	2.01	0.58	0.047	0.003	0.003	0.048	0.002	414	233
S6	0.71	2.14	0.57	0.53	0.003	0.006	0.041	0.002	401	221
S7	0.80	2.01	0.93	1.01	0.003	0.001	0.056	0.002	339	150

Austemperability evaluation

The austemperability was calculated through the D_{jm} distance. Along the Jominy test sample, each Jominy distance is characterised by a distinctive cooling rate for all steels. Figure 3 shows the cooling rate at 704°C as a function of Jominy distance [26]. In order to develop a relationship between hardenability and austemperability, numerical simulations were carried out with free software Elmer, in which round bars of 5–70 mm diameter were cooled down from 900°C (austenitising temperature) to several T_{IB} in the range 220–430°C.

The heat extraction of the molten salt bath largely affects the cooling rate of a sample submerged into the bath. The characterisation of the molten salt bath used in this study was made by means of the calculation of the heat transfer coefficient 'h'. For that purpose, the cooling curve of the centre of a ductile iron sphere was recorded by using a thermocouple. The samples were austenitised at 900°C and cooled into the molten salt bath (46% sodium nitrite and 54% potassium nitrate) held at 230, 320 and 370°C. The h coefficient was calculated on the basis of the temperature records and solving the inverse transient heat transfer for a sphere.

Then, the cooling rates at the centre of the bars were calculated at 704°C and compared with those corresponding to the D_{jm}. Those round bars having a cooling rate at their centres equal to or greater than that corresponding to the D_{jm} are assumed to be fully austemperable. The relationship between hardenability and austemperability was experimentally validated by the austempering of cylindrical pieces with different diameters and a length/diameter ratio greater than 3.

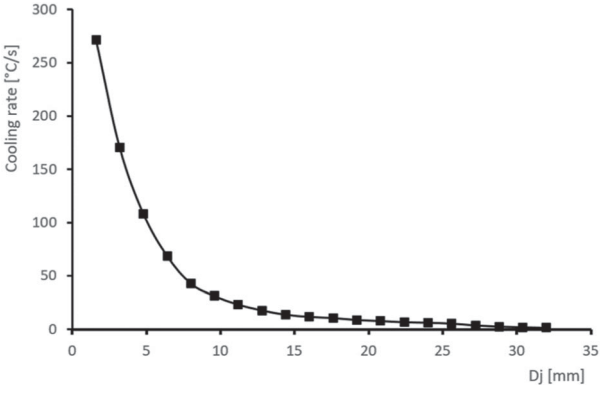

Figure 3. Cooling rate as a function of Jominy distance [26].

Results

Microstructures and Jominy curves

The Jominy hardness plots and the D_{jm} of the studied steels are shown in Figs. 4–11. Figure 4(A) shows the results for S1. After an initial plateau, the hardness drops from $D_j = 5$ mm. The microstructure of S1 along the Jominy distance is martensitic (Figure 4(B)) until it shows the precipitation of Widmanstätten ferrite at $D_{jm} = 5$ mm (Figure 5(A)) and pearlite at $D_j = 9$ mm (Figure 5(B)). As the D_j increases, the pearlite amount increases until a fully pearlitic microstructure is obtained. The precipitation of ferrite at $D_{jm} = 5$ mm matches well with the fall in the Jominy hardness curve. According to the criteria stated above, a $D_{jm} = 5$ mm will be adopted for the calculation of the austemperability of S1.

Figure 6(A) shows the Jominy curve for S2. The drop in the hardness value is observed between D_j of 6–9 mm. The microstructure of S2 showed the precipitation of allotriomorphic and Widmanstätten ferrite and pearlite at a $D_{jm} = 7$ mm (Figure 6(B)). Accordingly, a $D_{jm} = 7$ mm will be taken to calculate the austemperability of S2.

The Jominy curve of S3 (Figure 7(A)) showed a continuous decrease of hardness along the Jominy distance. Different from S1 and S2, the curve itself does not give a clear indication of the Jominy distance corresponding

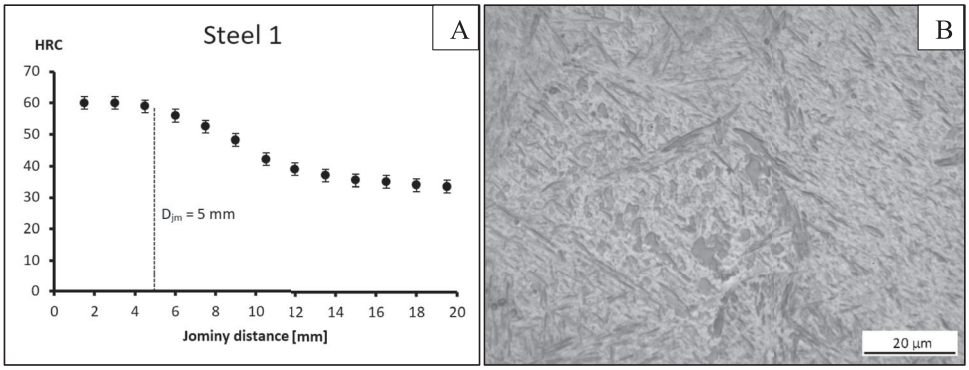

Figure 4. S1. Jominy curve (A). Martensitic microstructure in S1 for $D_j < 5$ mm (B).

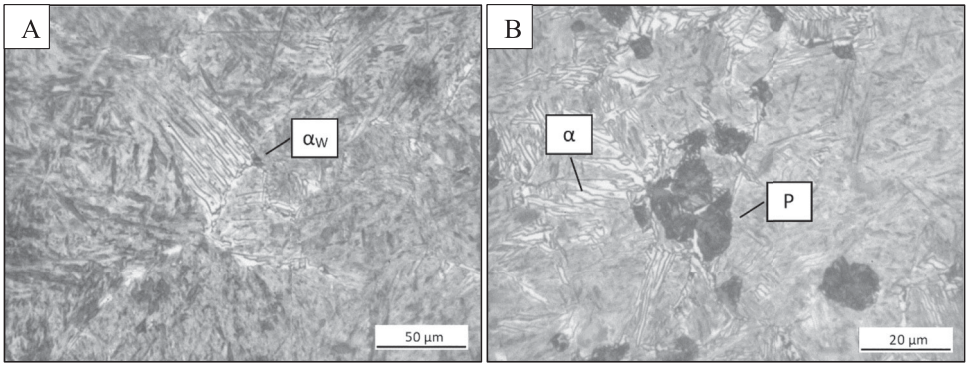

Figure 5. S1. Precipitation of Widmanstätten ferrite at $D_{jm} = 5$ mm (A). Precipitation of pearlite at $D_j = 9$ mm (B).

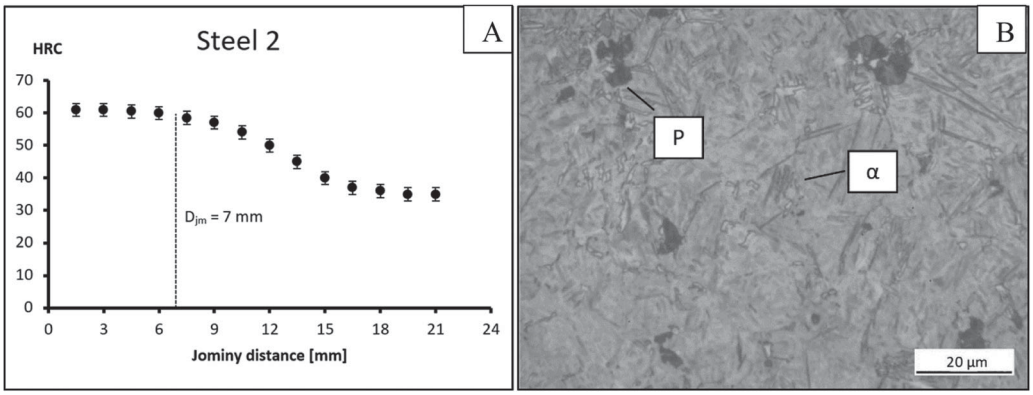

Figure 6. S2. Jominy curve (A). Ferrite and pearlite precipitation at $D_{jm} = 7$ mm (B).

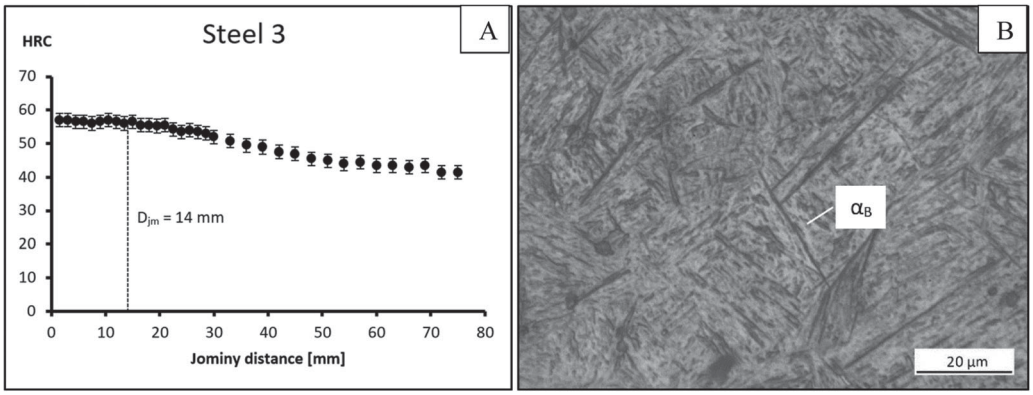

Figure 7. S3. Jominy curve (A). Precipitation of plates of bainitic ferrite at $D_{jm} = 14$ mm (B).

to the precipitation of unwanted phases. The microscopic examination showed that the first different-to-martensite phase observed in S3 was bainitic ferrite (Figure 7(B)). This behaviour is expected because S3 includes Mo, which causes a delay of the reconstructive transformations (as ferrite and pearlite) [27]. The bainitic ferrite was observed at a $D_{jm} = 14$ mm, mainly at first to freeze (FTF) zones, as these areas of the microstructure have lower concentration of alloying elements. It seems that the precipitation of bainitic ferrite causes a small drop in hardness that is difficult to notice on the Jominy plot.

S4 showed results similar to those observed for S3. The Jominy curve (Figure 8(A)) does not display a clear drop of the hardness. At $D_{jm} = 20$ mm, some plates of bainitic ferrite were observed in FTF zones (Figure 8(B)). The behaviour of S3 and S4 states the importance of identifying unwanted phases by means of metallographic observations when the Jominy curve does not show a clear drop of the hardness value.

It is important to state that in the case of S3 and S4, the first different-to-martensite phase observed along the specimens was bainite, a desirable phase when performing austempering heat treatments. However, the bainite obtained in the Jominy specimen was formed in continuous cooling. In that case, the bainite formed is not desirable, since the objective of an austempering heat treatment is to transform all the austenite into carbide-free bainite at a defined T_{IB}.

Figure 9(A) shows the curve of S5. The drop in hardness is observed at a D_j between 6 and 8 mm. The microstructure of S5 at a $D_{jm} = 7.5$ mm shows the simultaneous precipitation of ferrite (Widmanstätten and allotriomorphic) and pearlite in FTF zones (Figure 9(B)).

Figure 10A shows the Jominy curve for S6. It exhibits a fall of the hardness at about a $D_j = 12$ mm. The metallographic observation shows the precipitation of pearlite at $D_{jm} = 11$ mm (Figure 10(B)). Accordingly, a $D_{jm} = 11$ mm will be considered to calculate its austemperability.

S7 showed high hardenability, as shown by its Jominy curve (Figure 11A). The hardness remains constant until a $D_j = 30$ mm, making it possible to obtain a fully martensitic microstructure even at low cooling rates. The microstructure along the Jominy distance is martensitic until a $D_{jm} = 33$ mm, where the precipitation of pearlite occurs (Figure 11(B)) and produces a fall of the hardness. The great hardenability of this alloy was expectable due to the high contents of C, Mn and Cr in the steel chemical composition [12, 28, 29].

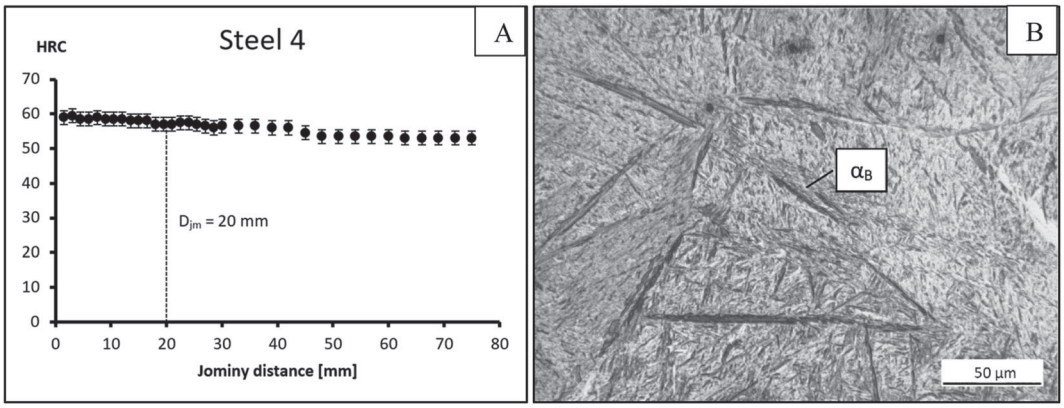

Figure 8. S4. Jominy curve (A). Precipitation of plates of bainitic ferrite at $D_{jm} = 20$ mm (B).

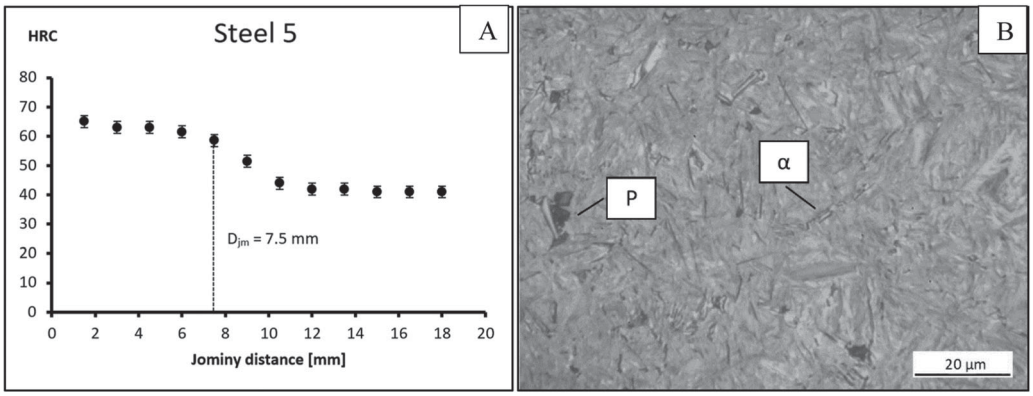

Figure 9. S5. Jominy curve (A). Precipitation of ferrite and pearlite at $D_{jm} = 7.5$ mm (B).

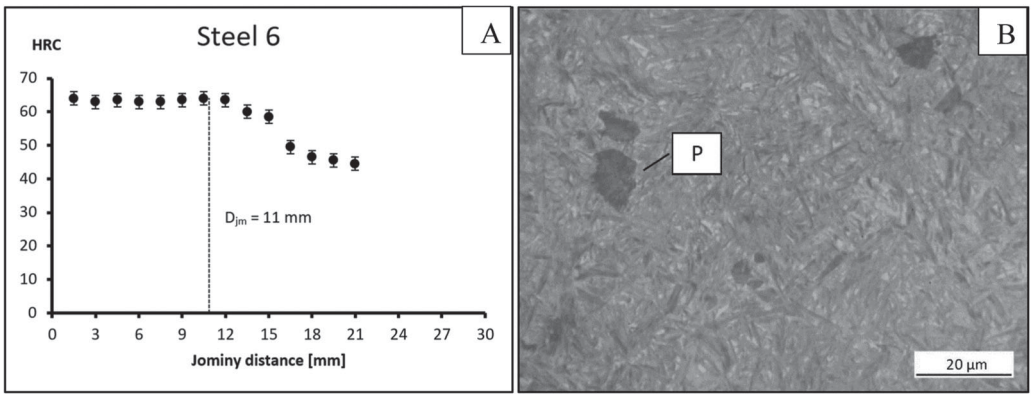

Figure 10. S6. Jominy curve (A). Precipitation of pearlite at $D_{jm} = 11$ mm (B).

Numerical simulations

Figure 12 shows the cooling curves of the centre of a 69 mm diameter sphere cooled in salt baths held at different temperatures. These curves were used to calculate the heat transfer coefficient h, assuming that h changes exponentially with the sample surface temperature following Equation (1). The best fit was obtained for the following constant values: $a = 170$ W m^{-2} °C^{-1}; $b = 0.0002$ W m^{-2} °C$^{-3.5}$ and $c = 2.5$. The heat transfer coefficient was found to be highly dependent on the sample surface temperature.

$$h\,(\mathrm{W\,m^{-}\,^{\circ}C}) = a + b \times T^{c} \qquad (1)$$

Figure 13 shows the cooling curves at the centre of two round bars of 10 and 70 mm diameter, calculated using the h coefficient expression when they cool down from 900 to 300°C. These curves were used to calculate the cooling rate at 704°C, temperature pointed by square symbols in the chart. It is important to state that the use of an austenitising temperature different from 900°C does not introduce significant changes in the cooling rates obtained at 704°C. Particularly, temperatures in the range 850–950°C lead to changes in the cooling rates of less than 1%. Therefore, the results obtained from the numerical calculations are valid for different austenitising temperatures.

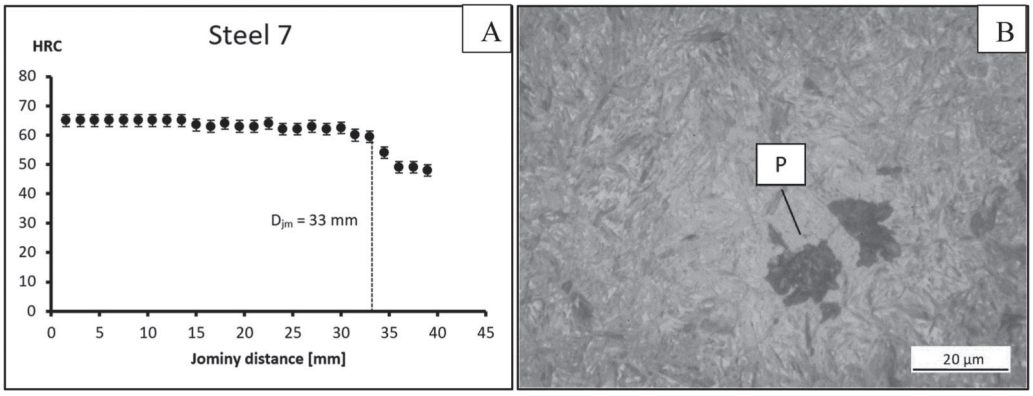

Figure 11. S7. Jominy curve (A). Precipitation of pearlite at $D_{jm} = 33$ mm (B).

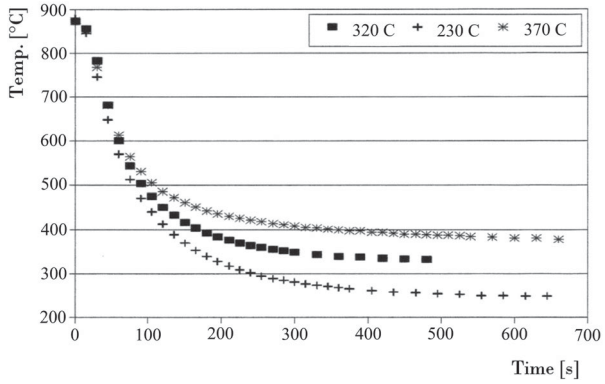

Figure 12. Cooling curves of the centre of spheres in salt baths at different temperatures.

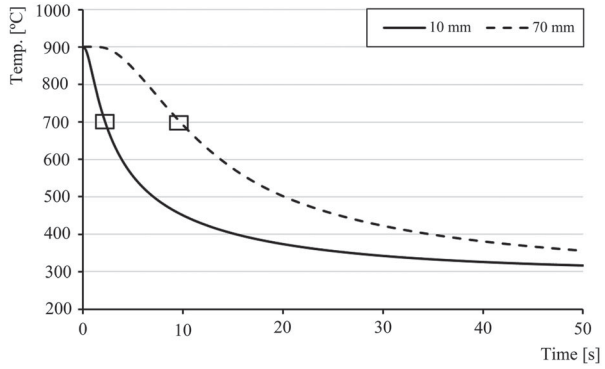

Figure 13. Cooling curves of 10 and 70 mm diameter round bars. $T_{IB} = 300°C$.

The calculated cooling rates for every combination of diameter and T_{IB} were compared with those shown in Figure 3 to obtain the relationship between round bar diameter, T_{IB} and Jominy distance. The relationship is plotted in Figure 14, where the correspondence between Jominy distance and round bars of different diameters, and for different temperatures of the molten salt bath is shown. For each D_j, the round bar diameter that has a similar cooling rate at its centre can be calculated for different salt bath temperatures. Therefore, those round bars having a cooling rate at their centres equal to or greater than that corresponding to its D_{jm} should become fully austempered after heat treatment. This method is applicable to steels in general, not just for high Si steels, since average thermal parameters of steels were applied in the numerical simulations. It also works for many austenitising temperatures. However, this plot is only applicable to the molten salt bath used in this study, composed of 46% sodium nitrite and 54% potassium nitrate.

Table 2. Calculated maximum austemperable diameters for a $T_{IB} = 300°C$.

	Steel 1	Steel 2	Steel 3	Steel 4	Steel 5	Steel 6	Steel 7
D_{jm}	5 mm	7 mm	14 mm	20 mm	7.5 mm	11 mm	33 mm
Φ_{Max}	9.5 mm	15 mm	36 mm	54 mm	16 mm	34 mm	> 70 mm

By means of the D_{jm} reported and the curves in Figure 14, the maximum austemperable diameters for the studied steels were calculated. For example, Table 2 shows the critical diameters for a $T_{IB} = 300°C$.

Experimental validation of the relationship between D_j and bar diameters

The relationship between bar diameters and Jominy distances presented in Figure 14 was validated by the austempering of round bars obtained from S2 keel blocks. The corresponding maximum austemperable

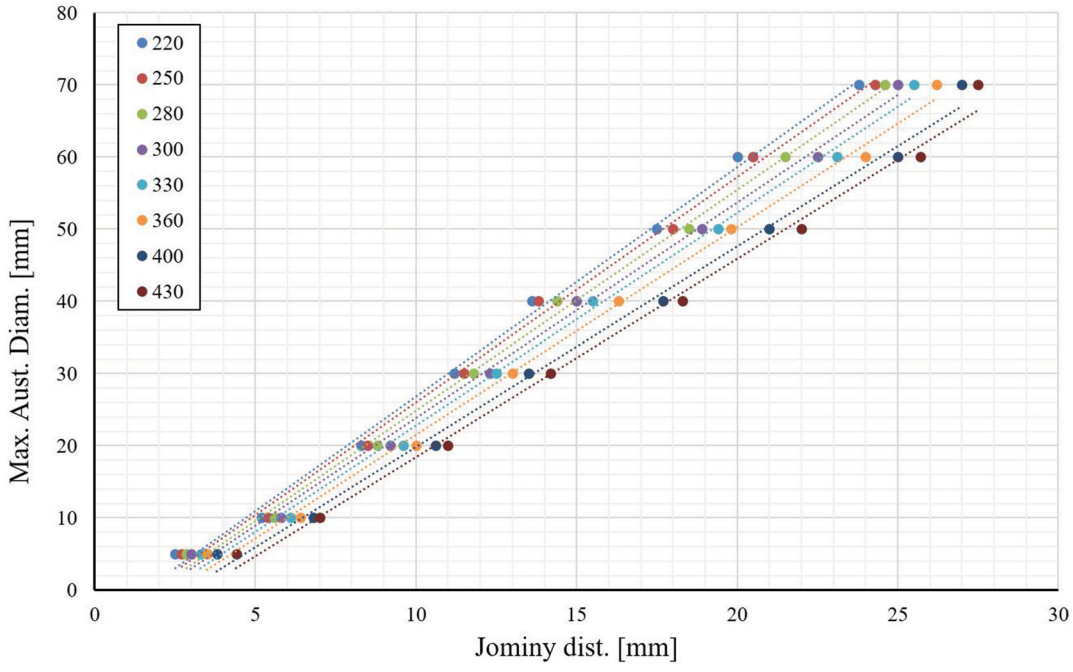

Figure 14. Relationship between austemperable diameter and Jominy distance, for different T_{IB}.

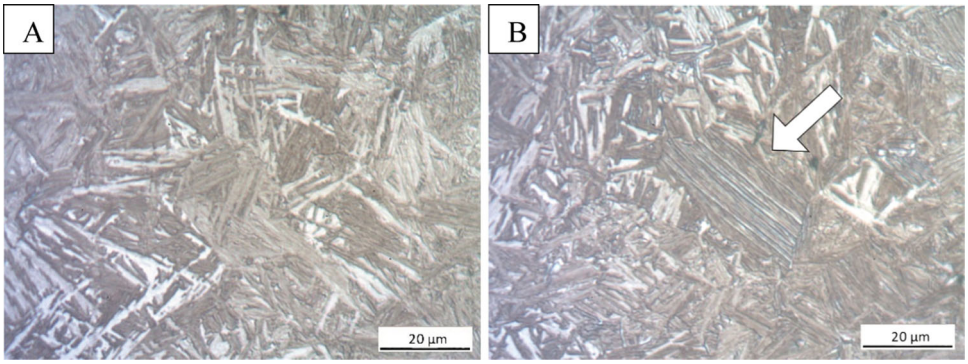

Figure 15. Validation. Rod of 13 mm diameter (A). Rod of 19 mm diameter (B).

diameter for S2 austempered at 280°C is 16 mm (see Table 2 and Figure 14). For that reason, cylinders with diameters of 13, 16 and 19 mm were prepared. The samples were austenitised at 900°C for 60 minutes and then austempered at 280°C for 3 hours.

The metallographic observation of the heat-treated samples shows that the 13 mm cylinder was fully austempered and its microstructure consists of plates of bainitic ferrite and retained austenite (Figure 15(A)). On the other hand, the sample of 16 mm diameter showed only very minor amounts proeutectoid ferrite, while 19 mm diameter sample showed noticeable precipitation of Widmanstätten and allotriomorphic ferrite at grain boundaries (Figure 15(B)), as was observed on the Jominy specimens. These experimental results validate the method proposed to evaluate austemperability from hardenability tests.

Discussion

Effect of alloy elements on austemperability

The austemperability results show that low-C and low-alloy steels, as S1, are adequate to obtain a fully bainitic microstructure only in thin section parts, due to its poor austemperability. As a benefit, this kind of steels has fast reaction kinetics, because of the low alloy content, which allows obtaining the desired microstructure rapidly [2,27]. However, if the aim is producing thicker pieces, it is necessary to include in the steels chemical composition a greater content of alloy elements.

The addition of C to the steels chemical composition is very effective to increase the austemperability. Adding 0.28 wt-% C raises the maximum austemperable diameter from 9.5 (S1) to 16 mm (S5) when austempering at 300°C. Cr is also very effective to increase the steels austemperability. Adding 0.5 wt-% Cr to medium-C steels raises the maximum austemperable diameter from 9.5 (S1) to 15 mm (S2) for a $T_{IB} = 300°C$. The effect of C and Cr additions combined is more effective than the individual additions. The addition of 0.17 wt-% C in a steel containing 0.5 wt-% Cr raises the austemperable diameter from 15 (S2) to 34 mm (S6).

The addition of 0.5 wt-% Cr in high-C steels increases the austemperable diameter from 16 (S5) to 34 mm (S6). The increased effectiveness of the combined addition of Cr and C on the hardenability of steels agrees with earlier reports [12,28,29].

The influence of C on steels austemperability is greater than that of Cr. Taking into account that C and Cr (together with Si and Mn, which influence was not studied in this work) are inexpensive alloy elements, Fe –C –Si –Mn –Cr systems seem to be a good choice for the design of steels intended to produce carbide-free austempered cast parts demanding high austemperability.

The addition of Ni and Mo in the steel chemical composition also causes a noticeable increase in the austemperability. However, the same effect can be achieved by alloying with C and Cr, at a lower cost. Moreover, the behaviour of S4 is interesting and requires special attention. It was expected the hardenability/austemperability of S4 to be lower than that of S3, since the inclusion of Al and Co in its chemical composition was supposed to accelerate solid-state transformations (as reported by Garcia-Mateo et al. [24]), causing a decrease in the steel austemperability. However, the results show that S4 has greater hardenability than S3. It is believed that the difference between the results of this work and those of Garcia-Mateós may be caused by the difference in the concentrations of Al and Co used in this work (0.6 and 0.3 wt-% respectively), that are lower than those used by Garcia-Mateo (1 and 1.5 wt-%).

This study shows that the austemperability of high Si cast steels austempered in a molten salt bath held at 300°C can change between 9 mm for unalloyed steels to more than 70 mm using low amounts of alloying elements. The procedure developed can be applied to calculate the austemperability of the same steels when different salt bath temperatures are used.

Comparison with austemperability of cast iron

Figure 16 shows a comparison of the correlation between Jominy distance and the centre of a round bar of a given diameter derived from this study, against the results obtained by Voigt et al. for cast iron [11],

using experimental data reported by BCIRA (British Cast Iron Research Association) [30]. Although steel and cast iron have different thermal properties, and the salt baths were not identical, there is a good coincidence in the results. In particular, the average slope of the lines is very similar. For example, a $D_j = 15$ mm corresponds to a diameter of 35 mm, according to this work, and a diameter of 33 mm according to Voigt´s study, for a $T_{IB} = 300°C$. However, Voigt 's results seem to present a higher dependency with T_{IB}, which could be attributed to differences in the composition of the salt bath.

Effect of microsegregation on the hardenability and austemperability

Because of the presence of microsegregation originated during solidification, the design of heat treatments for cast steels have to account for a non-uniform chemical composition. The microsegregation of steels 1, 3 and 4 w ere studied in a previous work [31] and it was concluded that every alloy element present in the alloys segregates to the last to freeze (LTF) zones, while FTF zones are alloy element depleted zones. This phenomenon causes that, when hardenability or austemperability limits are surpassed, the precipitation of high-temperature phases occurs first at FTF zones, where the lower concentration of alloying elements causes a higher critical cooling rate, i.e. the continuous cooling transformation (CCT) curves move to shorter times. This causes that, compared to rolled steels with the same chemical composition, cast steels have lower hardenability. This must be taken into account when designing chemical compositions for cast parts. The microsegregation effect is shown in Figure 17. Image A shows the precipitation of bainitic ferrite preferentially at FTF zones in S3 Jominy specimen at $D_j = 33$ mm, while image B shows the microstructure at $D_j = 17$ mm of S2, where the matrix is mainly pearlitic, but LTF zones are still martensitic.

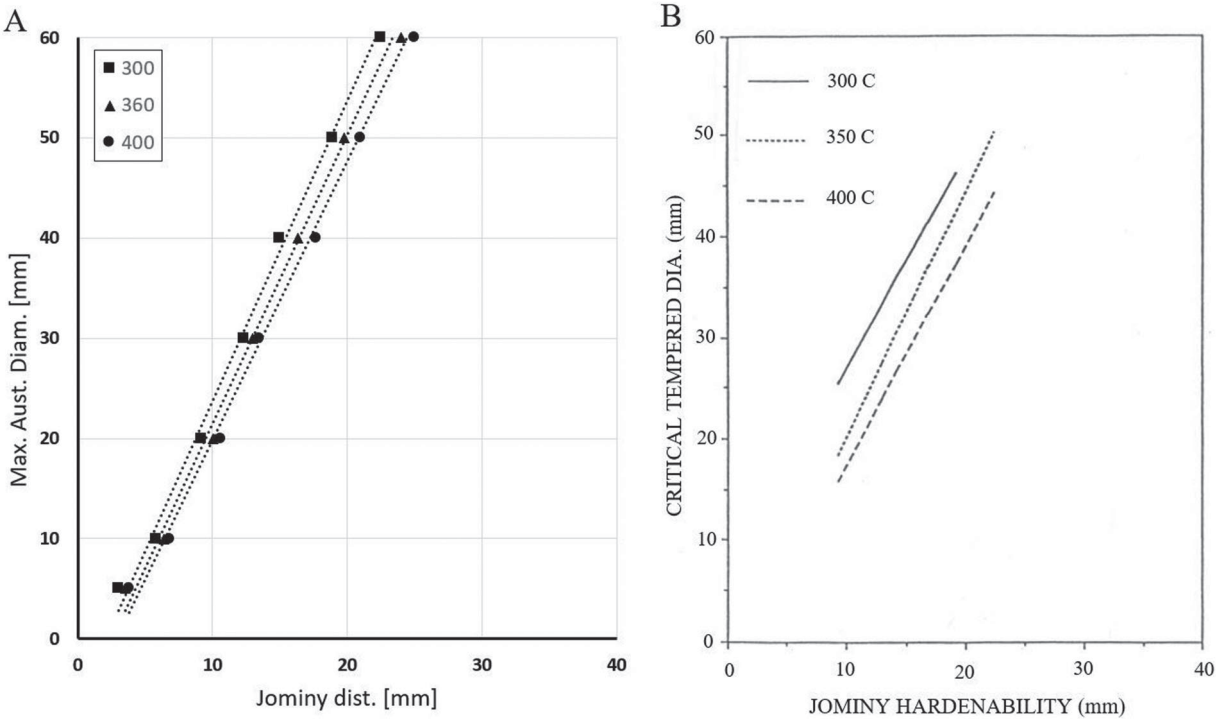

Figure 16. Comparison of results obtained in this work (A) with a similar work performed for Voigt for cast iron [11] (B).

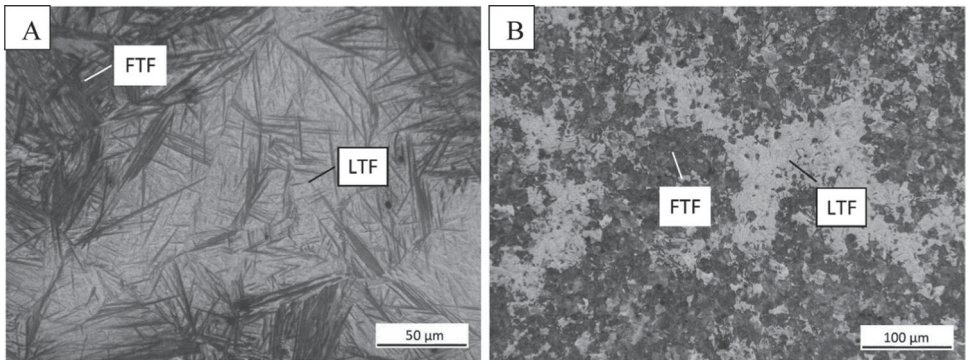

Figure 17. Effect of microsegregation in S3 (A) and S2 (B).

Conclusions

A procedure for determining the austemperability of steels by means of a Jominy end-quench test was developed. The procedure requires the metallographic observation of the microstructure along the length of a Jominy test sample. A chart, which allows calculating the maximum austemperable diameter as a function of the Jominy distance, was proposed and experimentally validated.

The austemperability of seven high silicon cast steels of different chemical compositions was characteri sed. It has been noticed that the microsegregation affects the steels hardenability since the unwanted higher-temperature phases precipitate first at FTF zones, which have low content of alloying elements. Microsegregation is detrimental to austemperability since, compared to rolled steels, cast steels of the same chemical composition will have lower hardenability and, in consequence, lower austemperability.

Finally, the influence of some alloy elements on the high Si steels austemperability was studied. It has been noticed that C and Cr are very effective at increasing the austemperability of these steels, particularly when used in combination. Other alloy elements as Ni and Mo also increase the steels austemperability, but the same effect can be reached using Cr and C at lower cost. In this manner, Fe –C –Si –Mn –Cr systems seem to be a good choice for producing cast parts with carbide-free bainitic microstructures at low cost.

Disclosure statement

No potential conflict of interest was reported by the authors.

Funding

This work was supported by ANPCyT and MINCyT of Argentina and Fondo para la Investigación Científica y Tecnológica [grant number PICT 12-1146 and PICT 14-3038].

ORCID

Nicolás Emanuel Tenaglia http://orcid.org/0000-0001-6372-8881
Roberto Enrique Boeri http://orcid.org/0000-0001-7083-579X
Juan Miguel Massone http://orcid.org/0000-0003-1287-1463

References

[1] Edmonds DV. Advanced bainitic and martensitic steels with carbide-free microstructures containing retained austenite. Mater Sci Forum. 2010;638–642:110–117.
[2] Caballero FG, Bhadeshia HKDH, Mawella DG, et al. Design of novel high strength bainitic steels: part 1. Mater Sci Technol. 2001;17:512–516.
[3] Caballero FG, Bhadeshia HKDH, Mawella DG, et al. Design of novel high strength bainitic steels: part 2. Mater Sci Technol. 2001;17:517–522.
[4] Avishan B, Yazdani S, Caballero FG, et al. Characterisation of microstructure and mechanical properties in two different nanostructured bainitic steels. Mater Sci Technol. 2014;31(12):1508–1520.
[5] Garcia-Mateo C, Caballero FG, Miller MK, et al. On measurement of carbon content in retained austenite in a nanostructured bainitic steel. J Mater Sci. 2012;47:1004–1010.
[6] Miihkinen VTT, Edmonds DV. Microstructural examination of two experimental high-strength bainitic low-alloy steels containing silicon. Mater Sci Technol. 1987;3:422–431.
[7] Kozeschnik E, Bhadeshia HKDH. Influence of silicon on cementite precipitation in steels. Mater Sci Technol. 2008;24(3):343–347.
[8] Peet MJ, Hill P, Rawson M, et al. Fatigue of extremely fine bainite. Mater Sci Technol. 2011;27(1):119–123.
[9] Garcia-Mateo C, Caballero FG, Sourmail T, et al. Tensile behaviour of a nanocrystalline bainitic steel containing 3 wt% silicon. Mater Sci Eng A. 2012;549:185–192.
[10] Carmo DJ, Dias JF, Santos DB. High cycle rotating bending fatigue property in high strength casting steel with carbide free bainite. Mater Sci Technol. 2011;28(8):991–993.
[11] Voigt RC, Lee YH, Tu C. Use of hardenability data to determine alloy requirements for austempered ductile iron. Proceedings of the 1991 World ADI Conference; 1991 March 12–14; Chicago (IL); 1991.
[12] Avishan B, Abdolalipour Asl Jani M, Yazdani S. Hardenability of nanocrystalline bulk steel. Trans Indian Inst Met. 2018;71(2):493–503.
[13] Peet MJ. Transformation and tempering of low-temperature bainite [dissertation]. Cambridge: University of Cambridge; 2010.
[14] Caballero FG, Bhadeshia HKDH, Mawella KJA, et al. Very strong low temperature bainite. Mater Sci Technol. 2002;18:279–284.
[15] Caballero FG, García-Mateo C, Miller MK. Modern steels at atomic and nanometre scales. Mater Sci Technol. 2015;31(7):764–772.
[16] Caballero FG, Poplawsky JD, Yen HW, et al. Complex nano-scale structures for unprecedented properties in steels. Mater Sci Forum. 2016;879:2401–2406.
[17] Sourmail T, Caballero FG, Garcia-Mateo C, et al. Evaluation of potential of high Si high C steel nanostructured bainite for wear and fatigue applications. Mater Sci Technol. 2013;29(10):1166–1173.
[18] Putatunda S. Austempering of a silicon manganese cast steel. Mater Manuf Processes. 2006;16(6):743–762.
[19] Chen X, Li Y. Effects of Ti, V, and Rare Earth on the mechanical properties of austempered high silicon cast steel. Metall Mater Trans A. 2006;37:3215–3220.
[20] Putatunda S. Influence of austempering temperature on microstructure and fracture toughness of a high-carbon, high-silicon and high-manganese cast steel. Mater Des. 2003;24:435–443.
[21] Mandal D, Ghosh M, Pal J, et al. Evolution of microstructure and mechanical properties under different austempering holding time of cast Fe–1.5Si–1.5Mn–V steels. Mater Des. 2014;54:831–837.
[22] Putatunda S. Fracture toughness of a high carbon and high silicon steel. Mater Sci Eng A. 2001;297:31–43.
[23] Li Y, Chen X. Microstructure and mechanical properties of austempered high silicon cast steel. Mater Sci Eng A. 2001;308:277–282.

[24] Garcia-Mateo C, Caballero FG, Bhadeshia HKDH. Acceleration of low-temperature bainite. ISIJ Int. 2003;43(11):1821–1825.
[25] Fernandino DO, Massone JM, Boeri RE. Characterization of the austemperability of partially austenitized ductile iron. J Mater Process Technol. 2013;213:1801–1809.
[26] Maroni PJ. Templabilidad: Un método para seleccionar aceros [Hardenability: a method for selecting steels]. Buenos Aires: Editorial Librería Mitre; 1976.
[27] Bhadeshia HKDH. Bainite in steels. London: IOM Communications Ltd; 2001.
[28] Cias WW, Doane DV. Phase transformational kinetics and hardenability of alloyed medium-carbon steels. Metall Trans. 1973;4:2257–2266.
[29] Doane DV. Application of hardenability concepts in heat treatment of steel. J Heat Treat. 1979;1(1):5–30.
[30] Blackmore PA, Harding RA. The effects of metallurgical process variables on the properties of austempered ductile irons. J Heat Treat. 1984;3(4):310–325.
[31] Tenaglia NE, Boeri RE, Basso AD, et al. Macro and microstructural characterisation of high Si cast steels – study of microsegregation patterns. Int J Cast Met Res. 2016;30(2):103–111.